Lower bound limit analysis using the Control Volume Finite Element Method

J.P. Hambleton & S.W. Sloan
University of Newcastle, Newcastle, NSW, Australia

A.V. Pyatigorets
ExxonMobil Upstream Research Company, Houston, TX, USA

V.R. Voller
University of Minnesota, Minneapolis, MN, USA

Abstract

The paper presents a novel approach for lower bound limit analysis based on the Control Volume Finite Element Method. The central concept of the solution procedure is a force balance on control volumes corresponding to nodes, where tractions on control volume faces are evaluated using linear interpolation of the unknown stress components at nodal points. An optimization routine incorporating second-order cone programming is subsequently employed to find the stress field that maximizes applied load subject to constraints imposed by equilibrium, boundary conditions, and the yield condition, thereby finding a load that is closest to the true collapse load. The formulation is for plain strain (i.e. two dimensions) and material obeying the Mohr-Coulomb yield condition. The proposed approach is applied to the benchmark problem of a uniform strip load applied to a half space, and very good agreement between analytical and numerical results is found.

1 INTRODUCTION

A large subset of problems in geotechnical and structural engineering pertains to analyzing the loads at which ultimate failure of the structure or underlying soil or rock occurs. Classical examples in geotechnical engineering are the bearing capacity of footings, earth pressure on retaining walls, and stability of slopes. In such stability problems, the primary quantity of interest is the limit load (i.e. collapse load) corresponding to incipient failure, with the history of displacements and stresses prior to failure being of secondary importance.

A variety of techniques are available to ascertain the limit load in structural and geotechnical problems. The four most prevalent approaches are (1) the lower and upper bound limit analysis methods, (2) the limit equilibrium method, (3) the method of characteristics (or slip-line method), and (4) the displacement-based Finite Element Method (FEM). Detailed descriptions of these approaches are given by Chen (1975).

Compared to the three other techniques listed above, upper and lower bound limit analysis methods are attractive for being simultaneously efficient, rigorous, and flexible in accommodating complex problem geometries and loading conditions. The limit equilibrium method, while capable of handling complex geometries and loads, can only be regarded as approximate. Conversely, the method of characteristics provides mathematically rigorous solutions but is prohibitively difficult to implement for all but the simplest problems. Displacement-based FEM is a tremendously powerful and flexible approach, though it suffers from being rather inefficient for limit load calculations. Namely, the solution procedure is predicated on incremental loading, such that the entire history of displacements and stresses leading up to failure must be evaluated in order to arrive at a prediction of the collapse load. Furthermore, the limit load is often not clearly defined, as in many cases the loads evaluated using FEM continually change even after a fully plastic mode of deformation reached.

The lower bound theorem for perfectly plastic materials obeying an associated flow rule states that, for a load *inducing* collapse, the true collapse load cannot be less than one evaluated from a stress field that (1) everywhere satisfies local equilibrium equations and boundary conditions and (2) nowhere violates the yield condition. By postulating a relatively simple stress field, a lower bound can be calculated analytically in some instances. In general, however, finding an admissible field is a non-trivial task, and a bound evaluated based on an overly simple stress field typically does not closely bracket the true limit load.

The central idea of numerical limit analysis is to split the problem domain into an arbitrary number of sub-domains (e.g. using FEM) in which the stress

field takes a simple form. In this way, the overall field can be arbitrarily complex and is thus capable of providing a bound close to the true collapse load. Numerical techniques for limit analysis have been researched extensively over the last several decades (e.g. Lysmer 1970, Anderheggen and Knöpfel 1972, Pastor 1978, Bottero et al. 1980, Sloan 1988, Zouain et al. 1993, Lyamin & Sloan 2002, Makrodimopoulos & Martin 2006), and these techniques are premised on finite element formulations that are essentially variations on the conventional finite element method.

In this paper, a novel approach for lower bound limit analysis based on the Control Volume Finite Element Method (CVFEM) is presented. The basis of the approach is to impose equilibrium via a force balance on control volumes within a generally unstructured mesh of linear finite elements, a concept originally proposed for solid mechanics problems by Fryer et al. (1991) and discussed in the monograph by Voller (2009). The primary advantages of CVFEM compared to other techniques are the relative simplicity of the method, the clear connection between the numerical procedure and the physics involved in the problem, and the potential for extension to multi-physics problems for which control volume methods are well-established (e.g. fluid flow and heat transfer). The specific case of plane strain and homogenous material obeying the Mohr-Coulomb yield condition is examined in this paper, although the approach can be extended to three-dimensional problems, alternative yield criteria, and inhomogeneous materials.

It is noted from the outset that the approach based on CVFEM only ensures a weak state of equilibrium (i.e. local equilibrium integrated over finite volumes), and it is therefore not clear whether computed loads can be regarded as mathematically rigorous lower bounds. This issue is discussed further in the concluding remarks (Section 4), after the numerical formulation has been described.

In the next section, details of the approach based on CVFEM are developed in full. In Section 3, the technique is verified by means of comparing numerical and analytical results for a benchmark problem.

2 NUMERICAL FORMULATION

2.1 Finite Element Mesh and Control Volumes

In the approach presented in this paper, the mesh consists of linear triangular elements, and control volumes are created around the vertices (nodes) using the construction described by Winslow (1966). A mesh of elements showing the control volume for a particular node i ($i = 1,2,...,N_{nodes}$, where N_{nodes} is the total number of nodes/control volumes) is depicted in Figure 1. The control volume is a polygon whose vertices are alternately the centroids of the supporting elements and the midpoints of element edges. Each node has N_{sup} supporting elements (e.g. $N_{sup} = 5$ in Fig. 1) that are identified using the index j ($j = 1,2,...,N_{sup}$) and numbered in an anticlockwise fashion. Using the local node numbering shown in Figure 1, the vertices of the control volume faces in the j^{th} supporting element are located at

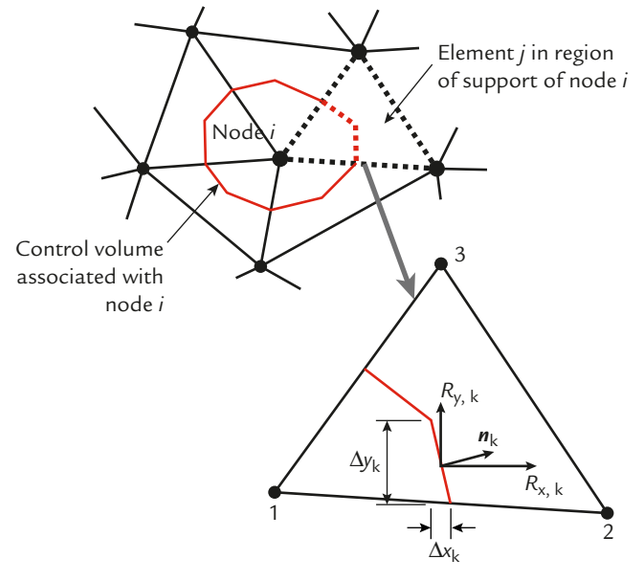

Figure 1 Control volume within finite element mesh and forces on control volume face.

$$x_{f,1} = \frac{1}{2}(x_1 + x_2),\ \ y_{f,1} = \frac{1}{2}(y_1 + y_2)$$
$$x_{f,2} = \frac{1}{3}(x_1 + x_2 + x_3),\ \ y_{f,2} = \frac{1}{3}(y_1 + y_2 + y_3) \qquad (1)$$
$$x_{f,3} = \frac{1}{2}(x_1 + x_3),\ \ y_{f,3} = \frac{1}{2}(y_1 + y_3)$$

In (1), $x_{f,p}$ and $y_{f,p}$ ($p = 1,2,3$) are the x- and y-coordinates, respectively, of the vertices of the control volume faces in anticlockwise order, and x_p and y_p are the coordinates of the nodal points.

A continuous stress field characterized by components σ_{xx}, σ_{yy} and σ_{xy} (compression negative) is obtained through linear interpolation of nodal values of stress, denoted $\sigma_{xx,p}$, $\sigma_{yy,p}$ and $\sigma_{xy,p}$ ($p = 1,2,3$). With the local numbering of nodes shown in Figure 1, the stress field can be expressed as

$$\sigma_{xx}(x,y) = \sum_{p=1}^{3} N_p(x,y)\sigma_{xx,p}$$
$$\sigma_{yy}(x,y) = \sum_{p=1}^{3} N_p(x,y)\sigma_{yy,p} \qquad (2)$$
$$\sigma_{xy}(x,y) = \sum_{p=1}^{3} N_p(x,y)\sigma_{xy,p}$$

where

$$N_1 = \frac{1}{2A}\left(x_2 y_3 - x_3 y_2 + y_{23} x + x_{32} y\right)$$
$$N_2 = \frac{1}{2A}\left(x_3 y_1 - x_1 x_3 + y_{31} x + x_{13} y\right)$$
$$N_3 = \frac{1}{2A}\left(x_1 y_2 - x_2 y_1 + y_{12} x + x_{21} y\right) \quad (3)$$
$$x_{32} = x_3 - x_2, \quad x_{13} = x_1 - x_3, \quad x_{21} = x_2 - x_1$$
$$y_{32} = y_2 - y_3, \quad y_{31} = y_3 - y_1, \quad y_{12} = y_1 - y_2$$
$$A = \frac{1}{2}\left|x_{13} y_{23} - x_{32} y_{31}\right|$$

2.2 Equilibrium Equations

Discrete equations of equilibrium are obtained by balancing forces on the faces of the control volume, allowing for body forces b_x and b_y in the x– and y-directions, respectively. Within the j^{th} element supporting node i, there are two control volume faces (lower right in Fig. 1). Moving in an anticlockwise direction, these faces are designated by $k = 1$ and $k = 2$, respectively. The normal of face k, denoted $\mathbf{n}_k$, has components $n_{x,k}$ and $n_{y,k}$ in the x- and y-directions, respectively, computed as

$$n_{x,k} = \frac{\Delta y_k}{l_k}, \; n_{y,k} = -\frac{\Delta x_k}{l_k}$$
$$\Delta y_k = \begin{cases} x_{f,2} - x_{f,1} \\ x_{f,3} - x_{f,2} \end{cases}, \; \Delta y_k = \begin{cases} y_{f,2} - y_{f,1} & \text{if } k = 1 \\ y_{f,3} - y_{f,2} & \text{if } k = 2 \end{cases} \quad (4)$$

where $l_k = (\Delta y_k^2 + \Delta y_k^2)^{1/2}$. Along the control volume face, components of traction in the x- and y-directions, denoted $t_{x,k}$ and $t_{y,k}$ respectively, are given by

$$t_{x,k}(x,y) = \sigma_{xx}(x,y) n_{x,k} + \sigma_{xy}(x,y) n_{y,k}$$
$$t_{y,k}(x,y) = \sigma_{xy}(x,y) n_{x,k} + \sigma_{yy}(x,y) n_{y,k} \quad (5)$$

As the stress field is linear within an element, the resultant force on a control volume face, whose components in the x- and y-directions are $R_{x,k}$ and $R_{y,k}$ respectively, is evaluated exactly by multiplying the value of stress at the center of the control volume face by the length of the face (i.e. single-point integration), viz.

$$R_{x,k} = l_k t_{x,k}(\bar{x}_k, \bar{y}_k)$$
$$R_{y,k} = l_k t_{y,k}(\bar{x}_k, \bar{y}_k) \quad (6)$$

where

$$\bar{x}_k = \begin{cases} \frac{1}{2}(x_{f,1} + x_{f,2}) \\ \frac{1}{2}(x_{f,2} + x_{f,3}) \end{cases}, \; \bar{y}_k = \begin{cases} \frac{1}{2}(y_{f,1} + y_{f,2}) & \text{if } k = 1 \\ \frac{1}{2}(y_{f,2} + y_{f,3}) & \text{if } k = 2 \end{cases} \quad (7)$$

For nodes on boundaries, the control volume is closed by joining the midpoints of the edges of the elements on the boundary directly to the node itself, as shown in Figure 2. Components of the resultant force acting on the first face of the boundary (keeping the anticlockwise convention) are denoted $T_{x,1}$ and $T_{y,1}$, and components on the second face are $T_{x,2}$ and $T_{y,2}$. These are evaluated in a similar manner as in (4–7).

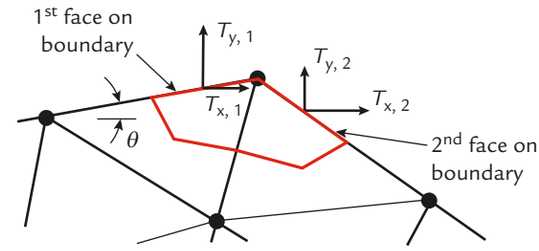

Figure 2 Control volume for node on boundary.

Finally, the two discrete equations of equilibrium for the control volume corresponding to node i can be expressed as

$$\sum_{j=1}^{N^s} \sum_{k=1}^{2} R_{x,kj} + T_{x,1} + T_{x,2} + A_{CV} b_x = 0$$
$$\sum_{j=1}^{N^s} \sum_{k=1}^{2} R_{y,kj} + T_{y,1} + T_{y,2} + A_{CV} b_y = 0 \quad (8)$$

where $R_{x,kj}$ and $R_{y,kj}$ are components of force on the k^{th} face of element j in the region supporting node i. In (8), contributions $T_{x,1}$, $T_{y,1}$, $T_{x,2}$, and $T_{y,2}$ are always zero for internal nodes, and A_{CV} is the area of the control volume calculated as

$$A_{cv} = \frac{1}{3} \sum_{j=1}^{N^s} A_j \quad (9)$$

where A_j is the area A of the j^{th} supporting element evaluated from (3).

2.3 Boundary Conditions

Tractions applied to the boundaries in general have a normal component t_n and shear component t_t. To be compatible with the piecewise linear stress field, t_n and t_t also vary linearly between nodes. In order that boundary conditions are enforced everywhere along the edge of a boundary element, it suffices to impose boundary conditions only at nodal points. This provides the following relationships, which must be satisfied at all boundary nodes

$$t_{n,i} = \sigma_{xx,i} \sin^2\theta + \sigma_{yy,i} \cos^2\theta - \sigma_{xy,i} \sin 2\theta$$
$$t_{t,i} = \frac{1}{2}(\sigma_{yy,i} - \sigma_{xx,i}) \sin 2\theta + \sigma_{xy,i} \cos 2\theta \quad (10)$$

where $t_{n,i}$ and $t_{t,i}$ are nodal values of t_t and t_n and θ is the angle at which the boundary segment is inclined from the horizontal, taking the anticlockwise direction as positive (Fig. 2).

2.4 Yield Condition

In addition to satisfying equilibrium and boundary conditions, the stress field must nowhere violate the

yield condition. With linear interpolation of stress components, requiring that the yield is not violated at nodal points is sufficient, as convexity of the yield surface ensures that the yield condition is not violated within elements. For the Mohr-Coulomb yield condition, this implies

$$\sqrt{\left(\sigma_{\mathrm{xx,i}}-\sigma_{\mathrm{yy,i}}\right)^2+4\sigma_{\mathrm{xy,i}}^2}+\left(\sigma_{\mathrm{xx,i}}+\sigma_{\mathrm{yy,i}}\right)\sin\varphi-2c\cos\varphi\le 0 \tag{11}$$

where $\sigma_{\mathrm{xx,i}}$, $\sigma_{\mathrm{yy,i}}$, and $\sigma_{\mathrm{xy,i}}$ are stress components at node i ($i=1,2,...,N_{\mathrm{nodes}}$), φ is the angle of internal friction, and c is cohesion.

2.5 Optimization

The objective in lower bound limit analysis is to maximize external loads subject to the equality constraints of (8) and (10) as well as inequality constraint (11) imposed by the yield condition. In this paper, optimization was performed using the Matlab toolbox SeDuMi (Sturm 1999), which efficiently solves optimization problems involving various types of constraints. As noted by Krabbenhøft et al. (2007), the inequality in (11) represents a so-called quadratic, second-order cone constraint of the following form

$$\rho_{1,\mathrm{i}}\ge\sqrt{\rho_{2,\mathrm{i}}^2+\rho_{3,\mathrm{i}}^2} \tag{12}$$

where $i=1,2,...,N_{\mathrm{nodes}}$ and

$$\begin{aligned}\rho_{1,\mathrm{i}}&=-\left(\sigma_{\mathrm{xx,i}}+\sigma_{\mathrm{yy,i}}\right)\sin\varphi+2c\cos\varphi\\ \rho_{2,\mathrm{i}}&=\sigma_{\mathrm{xy,i}}-\sigma_{\mathrm{yy,i}}\\ \rho_{3,\mathrm{i}}&=2\sigma_{\mathrm{xy,i}}\end{aligned} \tag{13}$$

To utilize a standard optimization routine such as SeDuMi, it is necessary to assemble (for all nodes $i=1,2,...,N_{\mathrm{nodes}}$) all equality constraints into the following matrix form

$$\boldsymbol{A}\boldsymbol{x}=\boldsymbol{b} \tag{14}$$

where

$$\boldsymbol{A}=\begin{bmatrix}\boldsymbol{A}_\sigma & \boldsymbol{0}\\ \boldsymbol{A}_\rho & \mathbf{I}\end{bmatrix},\ \boldsymbol{x}=\begin{bmatrix}\sigma\\ \rho\end{bmatrix},\ \boldsymbol{b}=\begin{bmatrix}\boldsymbol{b}_\sigma\\ \boldsymbol{b}_\rho\end{bmatrix}$$

$$\begin{aligned}\sigma&=\left[\sigma_{\mathrm{xx},1}\ \sigma_{\mathrm{yy},1}\ \sigma_{\mathrm{xy},1}\ \ldots\ \sigma_{\mathrm{xx,N_{nodes}}}\ \sigma_{\mathrm{yy,N_{nodes}}}\ \sigma_{\mathrm{xy,N_{nodes}}}\right]^{\mathrm{T}}\\ \rho&=\left[\rho_{1,1}\ \ \rho_{2,1}\ \ \rho_{3,1}\ \ldots\ \rho_{1,\mathrm{N_{nodes}}}\ \rho_{2,\mathrm{N_{nodes}}}\ \rho_{3,\mathrm{N_{nodes}}}\right]^{\mathrm{T}}\end{aligned} \tag{15}$$

Matrix $\boldsymbol{A}_\sigma$ and the vector $\boldsymbol{b}_\sigma$ are assembled from the coefficients and constants appearing in (8) and (10), and their sizes depend on the number of nodes on the boundary at which boundary conditions are enforced, as well as any other equality constraints that might be imposed for the particular problem being investigated (e.g. uniform tractions over part of the boundary). Likewise, $\boldsymbol{A}_\rho$ and $\boldsymbol{b}_\rho$ are assembled from the coefficients and constants in (13), and their sizes are $3N_{\mathrm{nodes}}\times 3N_{\mathrm{nodes}}$ and $3N_{\mathrm{nodes}}\times 1$, respectively.

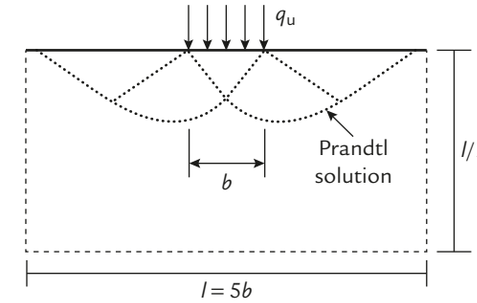

Figure 3 Rectangular region with uniform vertical stress q_u acting over segment of width b.

The matrices $\boldsymbol{0}$ and $\boldsymbol{I}$ in (15), sized appropriately, are a matrix of zeros and the identity matrix, respectively.

The "load" P to be maximized, whose physical interpretation depends on the problem under consideration, must be expressed as a linear combination of nodal values of stress in order to make use of a standard optimization routine, viz.

$$P=\boldsymbol{c}^{\mathrm{T}}\boldsymbol{x},\quad \boldsymbol{c}^{\mathrm{T}}=\left[c_1\ c_2\ \ldots\ c_{3\mathrm{N_{nodes}}}\ 0\ \ldots\ 0\right] \tag{16}$$

In many problems (e.g., bearing capacity and earth pressure), P is regarded as the integral of normal tractions over a part of the boundary $\partial\Omega$, and in this case the constants in **c** are evaluated from

$$P=-\sum\frac{L_{\mathrm{e}}}{2}\left(t_{\mathrm{n,r}}+t_{\mathrm{n,s}}\right) \tag{17}$$

where summation is over the element edges belonging to $\partial\Omega$, L_{e} is edge length of an element, and $t_{\mathrm{n,r}}$ and $t_{\mathrm{n,s}}$ are normal tractions at the two nodes belonging to an element, evaluated using (10). The negative sign in (17) appears because it is usually desirable to maximize a compressive load.

With **A**, **b**, and **c** defined by (15)–(17), the optimization problem can be written in the following canonical form used by standard optimization routines employing second-order cone programming

$$\begin{aligned}&\min -\boldsymbol{c}^{\mathrm{T}}\boldsymbol{x}\\ &\text{such that } \boldsymbol{A}\boldsymbol{x}=\boldsymbol{b}\\ &\qquad\rho_{1,\mathrm{i}}\ge\sqrt{\rho_{1,\mathrm{i}}^2+\rho_{2,\mathrm{i}}^2}\ \text{ for i}=1,2,...,N_{3,\mathrm{i\ nodes}}\end{aligned} \tag{18}$$

3 APPLICATION TO BENCHMARK PROBLEM

In this section the approach for lower bound limit analysis based on CVFEM is used to analyze the problem of a uniform normal traction applied over a segment of width b on a flat surface (Fig. 3). Considering weightless material, the analytical solution obtained by Prandtl (1921) for the limit load q_{u} using the method of characteristics (shown schematically in Fig. 3) is

$$q_{\mathrm{u}}=c\cot\varphi\left[\tan^2\left(\tfrac{\pi}{4}+\tfrac{\varphi}{2}\right)e^{\pi\tan\varphi}-1\right] \tag{19}$$

In the numerical approach, the domain is a rectangle of finite size, which has an assumed width $l=5b$

and height $l/2$ (Fig. 3). Also, it is assumed that shear tractions are zero on all boundaries, as this ensures that the stress field evaluated numerically can be extended throughout the entire semi-infinite domain.

In the numerical formulation employing a piecewise linear stress field, it is not possible to specify tractions that are precisely uniform. As illustrated in Figure 4, tractions at the outermost elements in the region of loading decrease linearly from q_u to 0. Nevertheless, the traction distribution will approach uniformity as the mesh refinement increases and $L_e/b \to 0$, where L_e is defined as the length of element edges along the boundaries.

Computations were performed using a uniform unstructured mesh constructed through Delaunay triangulation. The mesh and control volumes for $L_e/b = 1/2$ are shown in Figure 5.

Estimates of q_u with various levels of mesh refinement and $\varphi = 0$ are shown in Table 1. Also shown in the table are the total number of nodes N_{nodes} and the number of element N_e. With the coarse mesh corresponding to $L_e/b = 1/2$, the value of $q_u/c = 5.29$ using CVFEM in fact exceeds the value of $q_u/c = 2+\pi \approx 5.14$ from (19) as a result of non-uniform loading. When the element length is decreased, the load effectively becomes uniform, and the estimate of q_u/c approaches the value from the analytical solution from below. At $L_e/b = 8$, the limit load using CVFEM is only 2.4% less than the analytical result.

Figure 6 shows the optimal stress field corresponding to $L_e/b = 1/8$. As an added verification of the numerical results, it is seen that the field is essentially symmetric, though no symmetry conditions were imposed. Also, the variation of σ_{xx}/c resembles the stress field derived by Prandtl (1921) using the method of characteristics. This symmetric field, outlined schematically in Figure 3, consists of (1) a triangular region of uniform stress beneath the load, (2) two fans, and (3) two regions of uniform stress extending to the boundaries.

Numerically calculated lower bounds on q_u for several values of friction angle φ are given in Table 2. The limit loads predicted using CVFEM are reasonably close to the analytical results, with the difference increasing from 2.4% at $\varphi = 0$ to 17.3% at

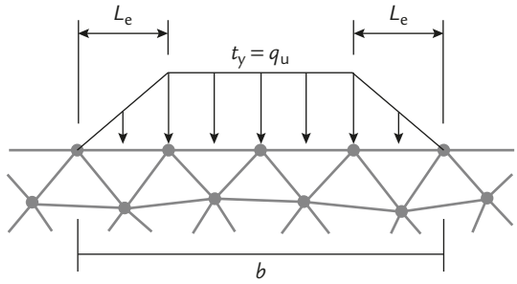

Figure 4 Tractions applied to boundary using CVFEM formulation with linear interpolation of nodal values.

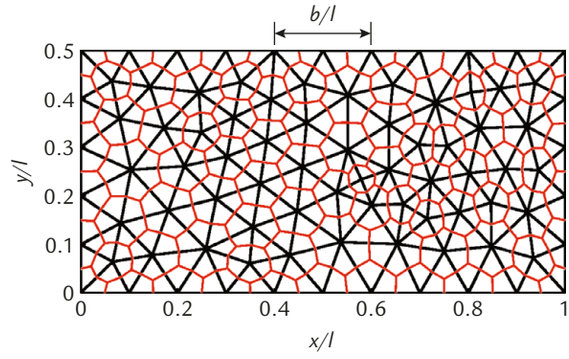

Figure 5 Unstructured finite element mesh showing control volumes ($L_e/b = 1/2$).

Table 1 Normalized average ultimate stress q_u/c for various levels of mesh refinement

L_e/b	N_e	N_{nodes}	q_u/c
1/2	142	87	5.29
1/4	572	317	4.84
1/8	2282	1202	5.02

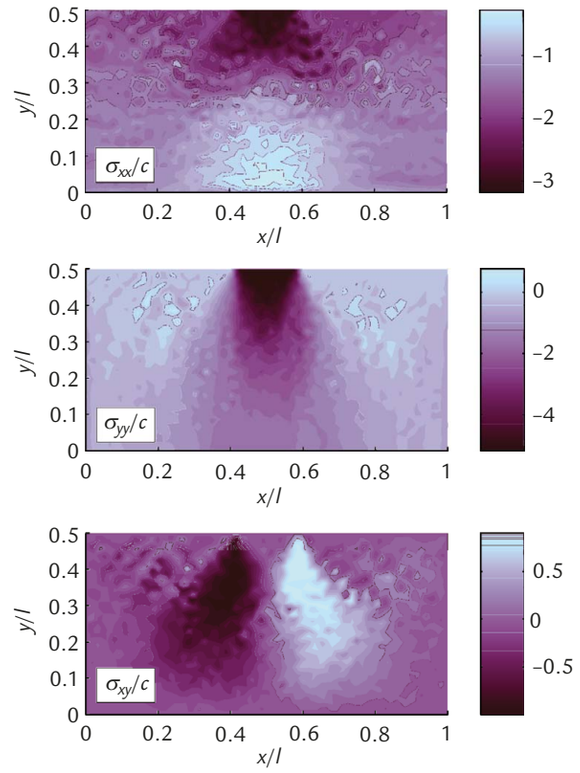

Figure 6 Optimal stress distribution for $\varphi = 0$ ($L_e/b = 1/8$).

Table 2 Normalized ultimate stress q_u/c for various values of friction angle φ compared with analytical solution ($L_e/b = 1/8$)

φ (deg)	q_u/c	
	CVFEM	Prandtl (1921)
0	5.02	5.14
10	7.94	8.35
20	13.7	14.8
30	27.1	30.1
40	66.3	75.3
50	221	267

$\varphi = 50°$. As in the analytical solution, numerical values of q_u/c sharply increase with increasing φ.

4 CONCLUDING REMARKS

The numerical approach for lower bound limit analysis presented in this paper utilizes CVFEM with a generally unstructured mesh of linear triangular elements to predict lower bounds on the plastic collapse load in structural and geotechnical engineering applications. Through comparison with a problem for which an analytical solution exists, it is demonstrated that the approach is capable of evaluating a lower bound that is close to the true collapse load.

As indicated in the introduction of the paper, the proposed method does not in general satisfy the local (i.e. differential) equilibrium equations, which would indicate that calculated loads cannot be interpreted as mathematically rigorous lower bounds. However, it may be possible to extend the piecewise linear stress field on the boundary of each control volume into its interior in such a way that local equilibrium and the yield condition are satisfied, in which case the loads evaluated would in fact represent rigorous bounds. It is also a requirement in semi-infinite domains to be able to extend the stress field throughout the entire domain. This is possible for the specific problem considered in Section 3, but it is not readily apparent how this can be achieved for arbitrary domains and problems involving body forces. These issues are not investigated here but rather left as items of future exploration.

While the formulation presented is for two-dimensional problems and linear triangular elements, it is also possible to apply CVFEM to three-dimensional problems and to use alternative types of elements (cf. Voller 2009). In addition, allowing for admissible stress discontinuities (c.f. Sloan 1988, Lyamin & Sloan 2002) would reduce the level of mesh refinement needed for an accurate solution, given that discontinuities can occur in the true stress field.

ACKNOWLEDGMENT

The first and second authors would like to acknowledge financial support provided by the Australian Research Council (grant number FL0992039) in the form of an Australian Laureate Fellowship awarded to Prof. Scott Sloan.

REFERENCES

Anderheggen, E. & Knöpfel, H. 1972. Finite element limit analysis using linear programming. *International Journal of Solids and Structures* 8(12): 1413–1431.

Bottero, A., Negre, R., Pastor, J. & Turgeman, S. 1980. Finite element method and limit analysis theory for soil mechanics problems. *Computer Methods in Applied Mechanics and Engineering* 22(1): 131–149.

Chen, W.F. 1975. *Limit Analysis and Soil Plasticity*. Amsterdam: Elsevier.

Fryer, Y.D., Bailey, C., Cross, M. & Lai, C.H. 1991. A control volume procedure for solving the elastic stress-strain equations on an unstructured mesh. *Applied Mathematical Modelling* 15(11–12): 639–645.

Krabbenhøft, K., Lyamin, A.V. & Sloan, S.W. 2007. Formulation and solution of some plasticity problems as conic programs. *International Journal of Solids and Structures* 44(5): 1533–1549.

Lyamin, A.V. & Sloan, S.W. 2002. Lower bound limit analysis using nonlinear programming. *International Journal for Numerical Methods in Engineering* 55(5): 573–611.

Lysmer, J. 1970. Limit analysis of plane problems in soil mechanics. *Journal of the Soil Mechanics and Foundations Division ASCE* 96(4): 1311–1334.

Makrodimopoulos, A. & Martin, C.M. 2006. Lower bound limit analysis of cohesive-frictional materials using second–order cone programming. *International Journal for Numerical Methods in Engineering* 66(4): 604–634.

Pastor, J. 1978. Analyse limits: détermination numérique des solution statiques complètes. Application au talus vertical. *Journal de Mécanique Appliquée* 2(2): 167–196.

Prandtl, L. 1921. Über die Eindringungs-festigkeit (Härte) plastischer Baustoffe und die Festigkeit von Schneiden. *Zeitschrift für Angewandte Mathematik und Mechanik* 1(1): 15–20.

Sloan, S.W. 1988. Lower bound limit analysis using finite elements and linear programming. *International Journal for Numerical and Analytical Methods in Geomechanics* 12(1): 61–77.

Sturm, J.F. 1999. Using SeDuMi 1.02, A Matlab toolbox for optimization over symmetric cones. *Optimization Methods and Software* 11(1): 625–653.

Voller, V.R. 2009. *Basic Control Volume Finite Element Methods for Fluids and Solids*. Singapore: World Scientific.

Winslow, A.M. 1966. Numerical solution of the quasilinear Poisson equation in a nonuniform triangle mesh. *Journal of Computational Physics* 1(2): 149–172.

Zouain, N., Herskovits, J., Borges, L.A. & Feijóo, R.A. 1993. An iterative algorithm for limit analysis with nonlinear yield functions. *International Journal of Solids and Structures* 30(10): 1397–1417.